

Structural and magnetic phase transitions in $\text{Na}_{1-\delta}\text{FeAs}$ Shiliang Li,^{1,2,*} Clarina de la Cruz,^{2,3} Q. Huang,⁴ G. F. Chen,^{5,1} T.-L. Xia,⁵ J. L. Luo,¹ N. L. Wang,¹ and Pengcheng Dai^{2,3,1,†}¹Beijing National Laboratory for Condensed Matter Physics and Institute of Physics, Chinese Academy of Sciences, P.O. Box 603, Beijing 100190, China²Department of Physics and Astronomy, The University of Tennessee, Knoxville, Tennessee 37996-1200, USA³Neutron Scattering Science Division, Oak Ridge National Laboratory, Oak Ridge, Tennessee 37831-6393, USA⁴NIST Center for Neutron Research, National Institute of Standards and Technology, Gaithersburg, Maryland 20899, USA⁵Department of Physics, Remin University of China, Beijing 100872, China

(Received 5 May 2009; revised manuscript received 18 June 2009; published 9 July 2009)

We use neutron scattering to study the spin and lattice structures of single crystal and powder samples of $\text{Na}_{1-\delta}\text{FeAs}$ ($T_c=23$ K). Upon cooling from room temperature, the system goes through a series of phase transitions: first changing the crystal symmetry from tetragonal to orthorhombic at 49 K, then ordering antiferromagnetically with a spin structure similar to that of LaFeAsO and a small moment ($0.09 \pm 0.04\mu_B$), and finally becoming superconducting below about 23 K. These results confirm that antiferromagnetic order is ubiquitous for the parent compounds of the iron arsenide superconductors and suggest that the separated structural and magnetic phase-transition temperatures are due to the reduction in the c -axis exchange coupling of the system.

DOI: 10.1103/PhysRevB.80.020504

PACS number(s): 75.25.+z

Determining the universal features of iron arsenide superconductors is an important first step in developing a microscopic theory to understand the high-transition temperature (high- T_c) superconductivity in these materials.¹ From the outset, it was known that antiferromagnetic (AF) order is a competing ground state to superconductivity in iron arsenide superconductors. The parent compound LaFeAsO exhibits a structural distortion at 155 K and then orders antiferromagnetically below 137 K; electron doping to induce superconductivity suppresses both the structural distortion and static AF order.^{2,3} Although subsequent neutron-scattering experiments on the parent compounds of other iron-based superconductors including $R\text{FeAsO}$ ($R=\text{Ce}, \text{Pr}, \text{Nd}$),⁴⁻⁷ AFe_2As_2 ($A=\text{Ba}, \text{Sr}, \text{Ca}$),⁸⁻¹⁰ and FeTe (Refs. 11 and 12) have found similar lattice distortion and AF order as that of the LaFeAsO , the $M\text{FeAs}$ system ($M=\text{Li}, \text{Na}$) seemed to be an exception to this universal picture since the initial neutron and x-ray scattering experiments have found no evidence of lattice distortion or static AF order.¹³⁻¹⁶ These results are in contrast with local-density approximation (LDA) calculations, where the Fermi surfaces and magnetic orders of $M\text{FeAs}$ are expected to be similar to that of the LaFeAsO .^{17,18} Although recent transport and heat-capacity measurements on single crystals of $\text{Na}_{1-\delta}\text{FeAs}$ showed two anomalies at 52 and 41 K that are assigned to structural and AF phase transitions, respectively,¹⁹ muon-spin rotation (μSR) experiments confirmed only the AF ordering and neutron scattering found no evidence for structural distortion.²⁰

In this Rapid Communication, we report neutron-scattering investigation of spin and lattice structures of single crystals and polycrystalline materials of $\text{Na}_{1-\delta}\text{FeAs}$. We identify a tetragonal to orthorhombic structural phase transition near 50 K and thus confirm the transport measurements.¹⁹ Although our neutron powder-diffraction measurements were unable to detect AF order due to the small Fe moment, single-crystal experiments using thermal triple-axis spectroscopy unambiguously confirmed an AF phase transition below 40 K and showed that the system

forms a collinear in-plane AF spin structure identical to other iron arsenides⁴⁻¹⁰ but doubling the unit cell along the c axis [Fig. 1(a) and 1(b)]. The ordered moment is by far the smallest in iron arsenides, being $0.09 \pm 0.04\mu_B$. These results suggest that AF order with a collinear in-plane spin structure is ubiquitous property of the parent compounds of iron arsenide superconductors. We argue that the separated structural and magnetic phase transitions in $\text{Na}_{1-\delta}\text{FeAs}$ is due to reduced c -axis exchange coupling and Na deficiencies. Bulk super-

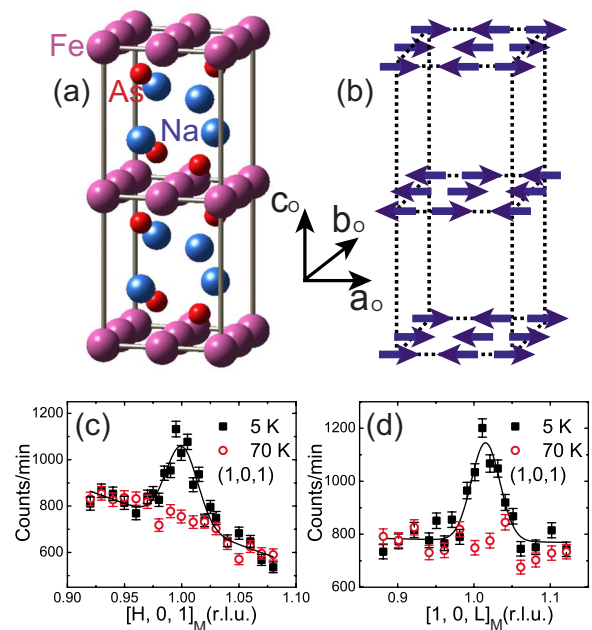


FIG. 1. (Color online) (a) Nuclear and (b) magnetic structures of the ideal NaFeAs . (a) includes two orthorhombic nuclear unit cells for comparison with the magnetic unit cell in (b). (c) and (d) show the $[H, 0, 1]$ and $[1, 0, L]$ scans around $(1, 0, 1)_M$ magnetic Bragg peak at 5 and 70 K. Both peaks disappear at 70 K, indicating their magnetic nature.

conductivity in $\text{Li}_{1-\delta}\text{FeAs}$ and $\text{Na}_{1-\delta}\text{FeAs}$ can only arise with enough self-doping induced by alkali-metal deficiencies.

We prepared 7 g of polycrystalline $\text{Na}_{1-\delta}\text{FeAs}$ sample and 0.6 g of single crystals as described in Ref. 19. The resistivity measurement on single crystals gives the onset and zero resistivity T_c as 23 and 8 K, respectively.¹⁹ We note that the properties between the powders and single crystals may be slightly different due to possibly different Na content. We thus only compare the results of detailed temperature dependence of nuclear and magnetic phase transitions on single crystals with the previous transport data.¹⁹ Powder neutron-diffraction measurements were performed on the BT-1 high-resolution powder diffractometer at the NIST Center for Neutron Research. The BT-1 diffractometer has a $\text{Ge}(3,1,1)$ monochromator ($\lambda=2.0785$ Å) and collimators with horizontal divergences of $15'-20'-7'$ full width at half maximum (FWHM). Powder-diffraction data refinement was done by using the GSAS program. The measurements on single crystals were carried out on the HB-1 triple-axis spectrometer at the High Flux Isotope Reactor, Oak Ridge National Laboratory. We fixed final neutron energy at $E_f=13.5$ meV and used (pyrolytic graphite) $\text{PG}(0,0,2)$ as monochromator and analyzer. The collimations for magnetic and structural measurements are $48'-60'-80'-120'$ and $15'-20'-20'-30'$, respectively. We denote $Q(\text{Å}^{-1})=(2\pi H/a, 2\pi K/b, 2\pi L/c)$, where $a_T=b_T=3.94481(3)$ Å and $c_T=6.99680(8)$ Å for tetragonal structure and $a_O=5.58906(8)$ Å, $b_O=5.56946(8)$ Å, and $c_O=6.9919(1)$ Å for orthorhombic structure. The magnetic unit cell is defined as $a_O \times b_O \times 2c_O$.

We first describe neutron powder-diffraction measurements. At a temperature well above the structural and magnetic phase transitions ($T=70$ K), Rietvelt analysis reveals a tetragonal structure with space-group $P4/nmm$ consistent with earlier results.²⁰ After cooling the sample down to 5 K, the tetragonal $(2,2,1)$ peak splits into two peaks as shown in Fig. 2(a). Detailed temperature dependence of the $(2,2,1)$ profiles in Fig. 2(a) reveals that the tetragonal to orthorhombic structural phase transition occurs near 45 K. Refinement of the diffraction pattern supports an orthorhombic structure at low temperature, and detailed structural parameters are listed in Table I for the two temperatures investigated. Fixing the occupancies of Fe and As to 1, we obtain the Na content as 0.985(7), or equivalently 1.5% Na deficiencies. Figures 2(b) and 2(c) show the temperature dependence of some key parameters. As a function of increasing temperature, the Fe-Fe bond length decreases until they become equal (tetragonal), while the Fe-As distance remains unchanged [Fig. 1(c)]. The orthorhombic lattice parameters a_O and b_O behave similarly [Fig. 1(b)]. While the nearest-neighbor bond angles change in opposite directions with increasing temperature, the diagonal bond angle is essentially temperature independent [Fig. 2(d)]. These results are similar to those of LaFeAsO (Ref. 21) and thus suggesting the same underlying mechanism for the structural phase transition.

To precisely determine the structural transition temperature, we carefully measured the temperature dependence of the $(1,1,0)_T$ peak width (in FWHM) on the single-crystal sample using $\lambda/2$ as shown in Fig. 3(a). Although the resolution of the triple-axis spectrometer is not good enough to

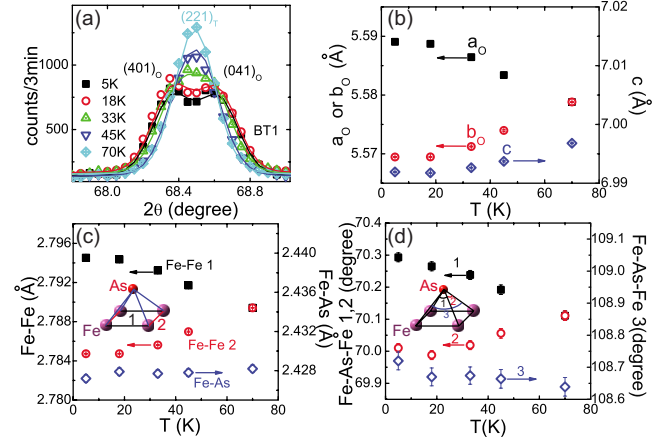


FIG. 2. (Color online) (a) Temperature dependence of the 2θ scans around the $(2,2,1)_T$ Bragg peak in powder-diffraction data across the tetragonal to orthorhombic phase transition. Clear splitting of the peaks is seen below 33 K. We collected full powder-diffraction spectra at several temperatures, and refinement results gave the temperature dependence of several key parameters: (b) lattice constants a , b , and c ; (c) bond lengths of Fe-Fe and Fe-As; and (d) bond angles of Fe-As-Fe. In all panels, left and right axes have the same scale.

resolve two separate peaks from the θ - 2θ scans at low temperature, the change in the FWHM reveals a structural phase-transition temperature of $T_O \approx 50$ K, which is consistent with the higher transition temperature in the transport measurements.¹⁹

To search for possible magnetic order, we carried out measurements using triple-axis spectroscopy on both the powder samples and single crystals. While we cannot find any magnetic peak in the powder-diffraction data due to small Fe moment, we observe clear AF order on single crystals at low temperatures. It turns out that the in-plane AF unit cell of $\text{Na}_{1-\delta}\text{FeAs}$ is identical to that of LaFeAsO ,² where the magnetic Bragg peaks are observed at $(1,0,L)_M$ ($L=1,3,5,7$). Figures 1(c) and 1(d) show wave-vector scans along the orthorhombic $[H,0,1]$ and $[1,0,L]$ directions⁶ at 5 and 70 K. The resolution limited peaks around $(1,0,1)_M$ at 5 K disappear at 70 K [Figs. 1(c) and 1(d)]. Figure 3(b) shows the temperature dependence of the scattering at wave vector $Q=(1,0,3)_M$, where we estimate that the onset magnetic transition temperature is about 37 K with less than 1 K thermal hysteresis [Fig. 3(b)]. These results are consistent with transport measurements where the ~ 40 K transition is identified as magnetic in nature. In a simple Ising model, the magnetic order parameter is related to temperature via $\phi(T)^2 \propto (1-T/T_N)^{2\beta}$. Fitting the whole temperature dependence of $(1,0,3)_M$ peak intensity yields an unreasonable $T_N=34.7 \pm 0.9$ K, shown as the black line in Fig. 3(b). Limiting the fitting range to temperatures above 20 K gives a $T_N=37.1 \pm 0.2$ K and $\beta=0.28 \pm 0.02$. However, we caution that the order parameter was measured using peak intensity on single crystals rather than integrated intensity measurement. We also note that the analysis of critical exponents is only valid over a very narrow temperature range close to the transition temperature.

A collinear AF structure could either have AF ordering

TABLE I. Refinement results of powder-diffraction data.

Na _{0.985} FeAs (5 K), <i>Cmma</i> , and $\chi^2=1.453$						
$a_O=5.58906(8)$ Å, $b_O=5.56946(8)$ Å, and $c_O=6.9919(1)$ Å						
Atom	Site	x	y	z	Occupancy	
Na	4a	0	0.25	0.3533(2)	0.985(7) ^a	
Fe	4g	0.25	0	0	1 ^b	
As	4a	0	0.25	0.7977(1)	1 ^b	

Selected bond lengths and angles:

Fe-Fe × 22.79453(4) Å	Fe-Fe × 22.78473(4) Å
Fe-As × 42.4272(4) Å	Na-As × 13.107(2) Å
Na-As × 22.9874(6) Å	Na-As × 22.9782(6) Å
Fe-As-Fe × 270.29(1)°	Fe-As-Fe × 270.01(1)°
Fe-As-Fe × 2108.72(3)°	

Na_{0.985}FeAs (70 K), *P4/nmm*, and $\chi^2=1.685$

$a_T=b_T=3.94481(3)$ Å, and $c_T=6.99680(8)$ Å						
Atom	Site	x	y	z	Occupancy	
Na	2c	0.25	0.25	0.3535(2)		
Fe	2a	0.75	0.25	0	1 ^b	
As	2c	0.25	0.25	0.7976(1)	1 ^b	

Selected bond lengths and angles:

Fe-Fe × 42.78941(3) Å	Fe-As × 42.4282(4) Å
Na-As × 42.9830(6) Å	Na-As × 13.107(2) Å
Fe-As-Fe × 470.11(2)°	Fe-As-Fe × 2108.64(3)°

^aNa occupancy is calculated as the mean value of those at several temperatures.

^bFe and As occupancies are fixed to 1.

directions along the *a* or *b* axis, which would correspond to magnetic peaks at $(1,0,L)_M$ or $(0,1,L)_M$ positions, respectively. In previous work on SrFe₂As₂,⁹ the AF ordering direction was determined to be along the *a*-axis direction by comparing the $(1,0,1)$ magnetic Bragg peak with $\lambda/2$ scattering from $(2,0,1)$ and $(0,2,1)$ nuclear Bragg peaks. Since the orthorhombic peak splitting in the case of Na_{1- δ} FeAs is rather small, we used very tight collimations for this purpose. Figure 4(a) shows the nuclear Bragg peak resulting from a superposition of the $(1,0,0.5)$ and $(0,1,0.5)$ peaks due to the twinned structure. It is immediately clear that the magnetic $(1,0,1)_M$ peak position in θ - 2θ scan is at a smaller 2θ angle than that of the nuclear peak, suggesting the magnetic structure propagates along the *a* axis. This result is consistent with earlier work on SrFe₂As₂.⁹

To determine the spin direction, we calculate the magnetic structure factors by assuming that the moments point to the *a*-axis direction. The observed magnetic intensities are obtained by integrating the θ - 2θ scans at the expected magnetic peak positions $(1,0,L)$ ($L=1,3,5,7$) in the three-axis mode. A comparison of the calculated and observed magnetic peak intensities shown in Fig. 4(b) reveals that such a model explains the data reasonably well. The small deviation between the observed and calculated intensities sets a limit of the moment direction to be within 15° away from the *a* axis.

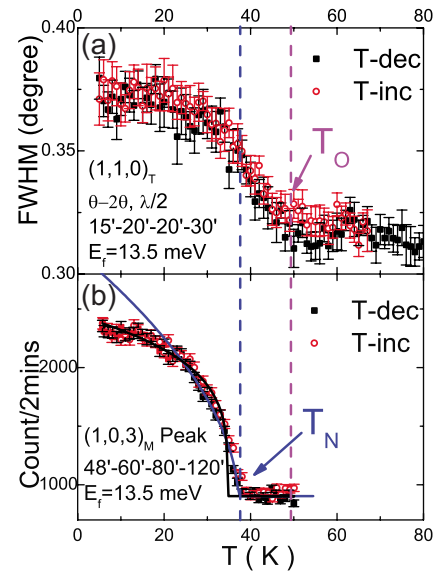


FIG. 3. (Color online) (a) Temperature dependence of the FWHM of θ - 2θ scan at the nuclear peak $(1,1,0)_T$ position using $\lambda/2$ scattering by removing the PG filter. The peak width clearly increases below about 50 K as marked by the vertical line. (b) Temperature dependence of the peak intensity at the AF peak $(1,0,3)_M$ position suggesting a Néel temperature of 39 K. The black line is the fitted result for the whole temperature range by using a simple Ising model described in the text, while the blue line only focuses on temperatures above 20 K which shows strong deviation from the experimental data below 20 K. No anomaly is seen across T_c , suggesting that superconductivity is filamentary and not a bulk phenomenon.

Therefore, the magnetic structure in Na_{1- δ} FeAs is the same as that in the AFFe₂As₂ system as shown in Fig. 1(b).⁸⁻¹⁰ Assuming this spin structure, we can estimate an Fe moment

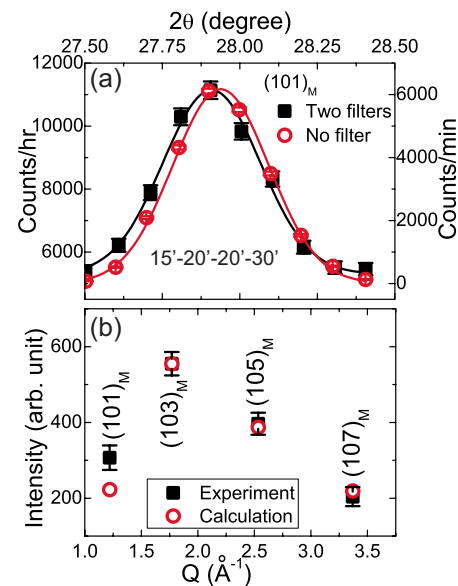


FIG. 4. (Color online) (a) Comparison of the θ - 2θ scans at $(1,0,1)_M$ with and without PG filter, measuring magnetic and nuclear peaks, respectively. (b) Calculated and experimental intensities of magnetic peaks $(1,0,L)_M$ ($L=1,3,5,7$). In the calculation, the moment is assumed to be along the a_O axis.

of $0.09 \pm 0.04 \mu_B$ by comparing intensities of the AF Bragg peaks with a series of nuclear peaks. Such a small moment explains why we as well as another group²⁰ cannot find any AF Bragg peaks in neutron powder-diffraction measurements.

Our results on $\text{Na}_{1-\delta}\text{FeAs}$ suggest that orthorhombic structure and collinear AF spin ordering in Fig. 1(b) are ubiquitous properties of undoped iron arsenides. Because of the difficulty in making stoichiometric samples of NaFeAs , Na deficiencies in the as-grown NaFeAs dope holes onto the FeAs plane that can induce superconductivity.¹⁹ For BaFe_2As_2 , transport and neutron-scattering experiments have shown that electron doping reduces the c -axis magnetic exchange coupling and separates the structural and magnetic phase transitions.^{22–25} Theoretically, it has been argued that the strength of the c -axis magnetic coupling controls the simultaneous or separated structural/magnetic phase transitions.²⁶ For lightly doped $\text{BaFe}_{1.96}\text{Ni}_{0.04}\text{As}_2$, inelastic neutron-scattering experiments showed a dramatic drop in the c -axis correlations with electron doping. Based on density function theory calculations, the c -axis exchange coupling of NaFeAs is smaller than that of BaFe_2As_2 but larger than that of LaFeAsO . Experimentally, the temperature separations between structural and magnetic phase transitions are similar for LaFeAsO^2 and NaFeAs . In addition, the AF order parameter showed no anomaly across T_c similar to those of $\text{BaFe}_{1.96}\text{Ni}_{0.04}\text{As}_2$ [Fig. 3(b)]. These results suggest that su-

perconductivity in our $\text{Na}_{1-\delta}\text{FeAs}$ is filamentary and not a bulk phenomenon. This is consistent with the fact that heat-capacity measurements show no observable anomaly near T_c in identically prepared samples.¹⁹ Since our single crystals of $\text{Na}_{1-\delta}\text{FeAs}$ are slightly doped away from ideal stoichiometry (Na deficiency), it is unclear whether the observed small moment and large differences in structural/magnetic phase-transition temperatures are the intrinsic or doping-induced c -axis coupling reduction. Future inelastic neutron-scattering experiments will be able to determine the exchange coupling along the c axis.

In conclusion, we have determined the lattice and magnetic structures of single-crystal $\text{Na}_{1-\delta}\text{FeAs}$. Our results indicate that the parent materials of NaFeAs and LiFeAs superconductors have orthorhombic lattice distortion and collinear AF order. This work establishes that the orthorhombic structure and AF collinear order are ubiquitous to all undoped iron arsenide materials. Superconductivity arises from electron or hole doping of their AF parent compounds and therefore suggests that spin fluctuations are important for superconductivity of these materials.

We thank Jiangping Hu, J. A. Fernandez-Baca, Tao Xiang, and Zhong-Yi Lu for helpful discussions. This work is supported by the U.S. NSF (Contract No. DMR-0756568), by the U.S. DOE BES (Contract No. DE-FG02-05ER46202), and by the U.S. DOE, Division of Scientific User Facilities. The work in IOP is supported by the CAS and MOST.

*slli@aphy.iphy.ac.cn

†daip@ornl.gov

¹Yoichi Kamihara, Takumi Watanabe, Masahiro Hirano, and Hideo Hosono, *J. Am. Chem. Soc.* **130**, 3296 (2008).

²C. de la Cruz *et al.*, *Nature (London)* **453**, 899 (2008).

³M. A. McGuire *et al.*, *Phys. Rev. B* **78**, 094517 (2008).

⁴J. Zhao *et al.*, *Nature Mater.* **7**, 953 (2008).

⁵S. A. J. Kimber, D. N. Argyriou, F. Yokaichiya, K. Habicht, S. Gerischer, T. Hansen, T. Chatterji, R. Klingeler, C. Hess, G. Behr, A. Kondrat, and B. Buchner, *Phys. Rev. B* **78**, 140503(R) (2008).

⁶J. Zhao *et al.*, *Phys. Rev. B* **78**, 132504 (2008).

⁷Y. Chen, J. W. Lynn, J. Li, G. Li, G. F. Chen, J. L. Luo, N. L. Wang, P. Dai, C. dela Cruz, and H. A. Mook, *Phys. Rev. B* **78**, 064515 (2008).

⁸Q. Huang, Y. Qiu, W. Bao, M. A. Green, J. W. Lynn, Y. C. Gasparovic, T. Wu, G. Wu, and X. H. Chen, *Phys. Rev. Lett.* **101**, 257003 (2008).

⁹J. Zhao, W. Ratcliff, J. W. Lynn, G. F. Chen, J. L. Luo, N. L. Wang, J. Hu, and P. Dai, *Phys. Rev. B* **78**, 140504(R) (2008).

¹⁰A. I. Goldman, D. N. Argyriou, B. Ouladdiaf, T. Chatterji, A. Kreyssig, S. Nandi, N. Ni, S. L. Budko, P. C. Canfield, and R. J. McQueeney, *Phys. Rev. B* **78**, 100506(R) (2008).

¹¹W. Bao, Y. Qiu, Q. Huang, M. Green, P. Zajdel, M. Fitzsimmons, M. Zhernenkov, M. Fang, B. Qian, E. Vohstedt, J. Yang, H. Pham, L. Spinu, and Z. Mao, *Phys. Rev. Lett.* **102**, 247001 (2009).

¹²Shiliang Li *et al.*, *Phys. Rev. B* **79**, 054503 (2009).

¹³X. C. Wang, Q. Q. Liu, Y. X. Lv, W. B. Gao, L. X. Yang, R. C. Yu, F. Y. Li, and C. Q. Jin, *Solid State Commun.* **148**, 538

(2008).

¹⁴M. J. Pitcher, D. R. Parker, P. Adamson, S. J. C. Herkelrath, A. T. Boothroyd, R. M. Ibberson, M. Brunelli, and S. J. Clarke, *Chem. Commun. (Cambridge)* (2008) 5918.

¹⁵J. H. Tapp, Z. Tang, B. Lv, K. Sasmal, B. Lorenz, P. C. W. Chu, and A. M. Guloy, *Phys. Rev. B* **78**, 060505(R) (2008).

¹⁶C. W. Chu *et al.*, *Physica C* **469**, 326 (2009).

¹⁷D. J. Singh, *Phys. Rev. B* **78**, 094511 (2008).

¹⁸R. Jishi and H. Alyahyaei, arXiv:0812.1215 (unpublished).

¹⁹G. F. Chen, W. Z. Hu, J. L. Luo, and N. L. Wang, *Phys. Rev. Lett.* **102**, 227004 (2009).

²⁰Dinah R. Parker, Michael J. Pitcher, Peter J. Baker, Isabel Franke, Tom Lancaster, Stephen J. Blundell, and Simon J. Clarke, *Chem. Commun. (Cambridge)* (2009) 2189.

²¹T. Nomura, S. W. Kim, Y. Kamihara, M. Hirano, P. V. Sushko, K. Kato, M. Takata, A. L. Shluger, and H. Hosono, *Supercond. Sci. Technol.* **21**, 125028 (2008).

²²N. Ni, M. E. Tillman, J. Q. Yan, A. Kracher, S. T. Hannahs, S. L. Budko, and P. C. Canfield, *Phys. Rev. B* **78**, 214515 (2008).

²³J.-H. Chu, J. G. Analytis, C. Kucharczyk, and I. R. Fisher, *Phys. Rev. B* **79**, 014506 (2009).

²⁴C. Lester, J. H. Chu, J. G. Analytis, S. C. Capelli, A. S. Erickson, C. L. Condon, M. F. Toney, I. R. Fisher, and S. M. Hayden, *Phys. Rev. B* **79**, 144523 (2009).

²⁵L. Harriger, A. Schneidewind, S. Li, J. Zhao, Z. Li, W. Lu, X. Dong, F. Zhou, Z. Zhao, J. Hu, P. Dai, arXiv:0904.3775 (unpublished).

²⁶C. Fang, H. Yao, W. F. Tsai, J. P. Hu, and S. A. Kivelson, *Phys. Rev. B* **77**, 224509 (2008).